

# Thermal Fractionalization of Quantum Spins in a Kitaev Model: Coherent Transport of Majorana Fermions and $T$ -linear Specific Heat

Joji Nasu,<sup>1</sup> Masafumi Udagawa,<sup>2</sup> and Yukitoshi Motome<sup>2</sup>

<sup>1</sup>*Department of Physics, Tokyo Institute of Technology, Ookayama, 2-12-1, Meguro, Tokyo 152-8551, Japan,*

<sup>2</sup>*Department of Applied Physics, University of Tokyo, Hongo, 7-3-1, Bunkyo, Tokyo 113-8656, Japan*

(Dated: December 3, 2024)

Finite-temperature ( $T$ ) properties of a Kitaev model defined on a honeycomb lattice are investigated by a quantum Monte Carlo simulation, from the viewpoint of fractionalization of quantum  $S = 1/2$  spins into two types of Majorana fermions, itinerant and localized. In this system, the entropy is released successively at two well-separated  $T$  scales, as a clear indication of the thermal fractionalization. We show that the high- $T$  crossover, which is driven by itinerant Majorana fermions, is closely related with the development of nearest-neighbor spin correlations. On the other hand, the low- $T$  crossover originates in thermal fluctuations of fluxes composed of localized Majorana fermions, by which the spectrum of itinerant Majorana fermions is significantly disturbed. As a consequence, in the intermediate- $T$  range, the system exhibits coherent transport of Majorana fermions and  $T$ -linear behavior in the specific heat, despite the Dirac semimetallic spectrum in the low- $T$  limit. We also show that the flux fluctuations affect the gapless-gapped phase boundary. Our results indicate that the fractionalization is experimentally observable in spin correlations, specific heat, and transport properties.

PACS numbers: 75.10.Kt, 75.70.Tj, 75.10.Jm

The fractionalization of electrons in solids into more fundamental degrees of freedom is one of the central topics in modern condensed matter physics. A prototypical example is found in one-dimensional strongly correlated electron systems: charge and spin degrees of freedom in an electron are separated and behave as independent particles termed holon and spinon [1]. In the insulating magnets with geometrical frustration, a different form of fractionalization is also anticipated to occur. For instance, the existence of the elementary excitation carrying a half of spin, named spinon, is predicted in a quantum spin liquid (QSL) [2–4], and emergence of magnetic monopoles is suggested in spin ice systems [5]. Another fractionalization was pointed out in heavy fermion systems as well. The half residual entropy in the two-channel impurity Kondo system is understood from the fractionalization of  $S = 1/2$  impurity spin into two Majorana fermions [6].

A quantum spin model, called the Kitaev model, has recently attracted considerable attention in broad areas of research, not only condensed matter physics but also statistical physics and quantum information [7]. This model is composed of  $S = 1/2$  spins with bond-dependent interactions on a honeycomb lattice. Such peculiar interactions were suggested to be realized in the systems with strong spin-orbit coupling, such as iridium oxides [8]. The most striking feature of this model is that it is exactly solvable due to the existence of  $Z_2$  conserved quantity on each hexagon, termed flux. The ground state dictates both gapless and gapped QSL phases depending on the exchange coupling constants. The exact solution is provided by representing  $S = 1/2$  spins by two types of Majorana fermions: one is localized and composes the fluxes, and the other forms itinerant bands [9–11]. The latter itinerant Majorana fermions determine the excitation spectrum in the QSLs. Thus, the fractionalization of spins into Majorana fermions is not just a mathematical tool but physically important in the Kitaev model.

A natural question arising here is how high-temperature ( $T$ ) paramagnetic spins are fractionalized into Majorana fermions when cooling the system. In one-dimensional electron systems, the spin-charge separation plays a key role in explaining their thermodynamic properties, in particular, in comparison with experiments. The thermodynamic properties in the Kitaev model and its extensions have also been studied, mainly for explaining the magnetism in iridium oxides [12–17], but the signature of fractionalization at finite  $T$  was not addressed in most of the previous studies. Among them, however, the authors pointed out the significance of fractionalization in a peculiar phase transition at finite  $T$  in a three-dimensional extension of the Kitaev model [15, 16]: the phase transition is governed by thermal excitations of localized Majorana fermions. Nevertheless, the relevance of fractionalization remains unclear, in particular, to the experimentally-observable quantities, such as the specific heat, spin correlations, and transport properties.

In this Letter, we investigate the effect of fractionalization of quantum spins on the finite- $T$  properties of the Kitaev model on a honeycomb lattice by applying the unbiased quantum Monte Carlo (QMC) method. In this model, the two Majorana fermions, itinerant and localized, release their entropy successively at two well-separated  $T$  scales. We elucidate that each crossover has an impact on experimental observables: the high- $T$  one, driven by itinerant Majorana fermions, corresponds to the development of spin correlations between neighboring sites, while the low- $T$  one, originating from thermal fluctuations of localized Majorana fermions, is accompanied by a sizable change in the excitation spectrum of itinerant Majorana fermions. This leads to coherent transport of Majorana fermions and apparent  $T$ -linear behavior of the specific heat in the intermediate  $T$  state with well-developed spin correlations, in contrast to the Dirac semimetallic behavior and  $T^2$  specific heat anticipated in the low- $T$  limit. Moreover, we

show that the thermal excitation of fluxes tends to open a gap at finite  $T$  near the gapless-gapped phase boundary.

The Kitaev model is composed of  $S = 1/2$  spins defined on a honeycomb lattice, whose Hamiltonian is given by

$$\mathcal{H} = -J_x \sum_{\langle jk \rangle_x} \sigma_j^x \sigma_k^x - J_y \sum_{\langle jk \rangle_y} \sigma_j^y \sigma_k^y - J_z \sum_{\langle jk \rangle_z} \sigma_j^z \sigma_k^z, \quad (1)$$

where  $\sigma_j^l$  is the  $l (= x, y, z)$  component of the Pauli matrix representing an  $S = 1/2$  spin at site  $j$ . Corresponding to three inequivalent bonds on the honeycomb lattice, named  $x$ ,  $y$ , and  $z$  bonds, the sum over  $\langle jk \rangle_l$  is taken over the nearest neighbor (NN) sites on the  $l$  bonds. The ground state of the model was exactly shown to be gapped and gapless QSLs depending on the exchange parameters,  $J_x$ ,  $J_y$ , and  $J_z$  [7] [see the inset of Fig. 1(p)]. The spin correlations are extremely short-ranged, i.e., nonzero only for the NN pairs [18–20]. The model does not exhibit any phase transition at finite  $T$  although a three-dimensional variant does [16].

We study the finite- $T$  properties of the model in Eq. (1) by the QMC method developed by the authors recently [16]. The method is based on the Majorana representation of the model via the Jordan-Wigner transformation along the chains consisting of the  $x$  and  $y$  bonds [9–11]. The Hamiltonian is rewritten in terms of two Majorana fermions  $c_j$  and  $\bar{c}_j$  as  $\mathcal{H} = iJ_x \sum_{\langle jk \rangle_x} c_j c_k - iJ_y \sum_{\langle jk \rangle_y} c_j c_k - iJ_z \sum_{\langle jk \rangle_z} \eta_r c_j c_k$ , where  $j < k$  is satisfied on the NN bonds. The operator  $\eta_r = i\bar{c}_j \bar{c}_k$ , which is defined on each  $z$  bond ( $r$  is the bond index), is regarded as a classical variable taking  $\pm 1$  because of  $[\mathcal{H}, \eta_r] = 0$  and  $\eta_r^2 = 1$  for all  $r$ . This representation allows us to carry out the QMC simulation without the negative sign problem. In the present calculations, we performed the MC simulation hybridized with the parallel tempering technique with 16 replicas [21] and spent the 10,000 MC steps for thermalization and 40,000 MC steps for measurement in up to an  $L = 12$  cluster, which contains  $N = 2 \times L^2 = 288$  sites.

Figures 1(a)-1(d) show the specific heat  $C_v$  as a function of  $T$  for several values of the anisotropy parameter  $\alpha$ ; here we define  $J_x = J_y = \alpha/3$  and  $J_z = 1 - 2\alpha/3$  so that  $J_x + J_y + J_z = 1$ . For all cases, the specific heat exhibits two peaks; both are almost system-size independent, indicating two crossovers. We hereafter term the low- and high- $T$  crossover temperatures as  $T_L$  and  $T_H$ , respectively. The entropy per site is shown in Figs. 1(e)-1(h). This rapidly decreases with decreasing  $T$  in the vicinity of  $T_L$  and  $T_H$  corresponding to the two peaks of the specific heat. A half of the entropy is released successively in each crossover; consequently, the entropy becomes  $\sim \frac{1}{2} \ln 2$  per site in the region between  $T_L$  and  $T_H$ . The plateau-like behavior of the entropy in this region becomes clearer for smaller  $\alpha$ , i.e., larger anisotropy of the exchange constants.

Let us discuss the origins and consequences of the two crossovers. First, we focus on the crossover at  $T_H$ . The itinerant Majorana fermions  $c_j$  form a band whose width is  $W_B = 2(J_x + J_y + J_z) - \Delta = 2 - \Delta$ , where  $\Delta$  is the excitation gap in the gapped phase. Suppose that the system is

in the gapless region and the density of states (DOS) is constant  $\sim 1/W_B$ , the specific heat originating from the itinerant Majorana fermions takes maximum at  $T \sim 0.511$ . This value well coincides with  $T_H$  in a wide region of  $\alpha$  including the gapped region. The result clearly indicates that the high- $T$  crossover originates in the itinerant Majorana fermions.

We find that the crossover at  $T_H$  is closely related with the development of NN spin correlations, which is experimentally observable. In the Kitaev model, the spin correlation  $\langle \sigma_j^l \sigma_k^l \rangle$  is nonzero only for the NN  $\langle jk \rangle_l$  bond [18]. Thus, we measure the equal-time spin correlation by  $S^l = \frac{2}{N} \sum_{\langle jk \rangle_l} \langle \sigma_j^l \sigma_k^l \rangle$ . The  $T$  dependences of  $S^l$  are presented in Figs. 1(i)-1(l) for the same set of  $\alpha$  as in Figs. 1(a)-1(h). Our QMC data obey the Curie behavior  $\sim \beta J_l$  at high  $T$ , indicated by the dashed-dotted curves in Figs. 1(i)-1(l). In the crossover region near  $T_H$ , however, the spin correlations show deviations from the Curie behavior, and quickly saturate to the values that are analytically obtained for the ground state (horizontal dashed lines in the figures). Hence, the high- $T$  crossover by the itinerant Majorana fermions corresponds to physically important behavior in this quantum spin system: the growth of the NN spin correlations.

Next, we discuss what occurs in the low- $T$  crossover. The entropy release near  $T_L$  originates from the localized Majorana fermions  $\bar{c}_j$  or  $\eta_r$ . This is confirmed by calculating the  $T$  dependence of the flux composed of the localized Majorana fermions  $\bar{c}_j$  as  $W_p = \prod_{r \in p} \eta_r$ , where  $p$  denotes the hexagonal plaquette in the honeycomb lattice. The thermal average of the flux density,  $W = \frac{2}{N} \sum_p \langle W_p \rangle$ , is presented in Figs. 1(e)-1(h). The results show that  $W$  rapidly decreases from 1 with increasing  $T$  in the vicinity of  $T_L$ . Hence, the crossover at  $T_L$  is due to the thermal fluctuation of fluxes.

The crossover behavior is summarized in Fig. 2. The phase diagram is divided into three regions: the high- $T$  paramagnetic region for  $T \gtrsim T_H$ , the intermediate- $T$  region for  $T_L \lesssim T \lesssim T_H$  where quantum spins develop NN correlations while the fluxes remain disordered, and the low- $T$  region for  $T \lesssim T_L$  where fluxes are aligned uniformly. While  $T_H$  is almost constant,  $T_L$  strongly depends on  $\alpha$ . We note that  $T_L$  in the small  $\alpha$  region well agrees with the asymptotic form in the anisotropic limit  $\alpha \rightarrow 0$  (toric code limit), where the effective two-level model leads to  $T_L \simeq 0.833 J_x^2 J_y^2 / (16 J_z^3)$  (the dashed curve in Fig. 2).

Since the  $Z_2$  variables  $\eta_r$  couple with the itinerant Majorana fermions, we expect that the enhanced fluctuations of fluxes above  $T_L$  affect the nature of itinerant Majorana fermions considerably. In order to elucidate such behavior, we calculate the DOS of itinerant Majorana fermions. The DOS with a given configuration of  $\eta_r$  is calculated by  $D(\omega, \{\eta_r\}) = \sum_n \delta(\omega - E_n(\{\eta_r\}))$ , where  $E_n$  is the one-particle energy of the fermion  $f_n$  which is introduced so as to diagonalize the Hamiltonian as  $\mathcal{H}(\{\eta_r\}) = \sum_n E_n(\{\eta_r\}) (f_n^\dagger f_n - \frac{1}{2})$ . The thermal averages of the DOS,  $\langle D(\omega) \rangle$ , are calculated for  $\{\eta_r\}$  generated in the QMC simulation. Note that  $\langle D(\omega) \rangle$  do not contain the  $T$  depen-

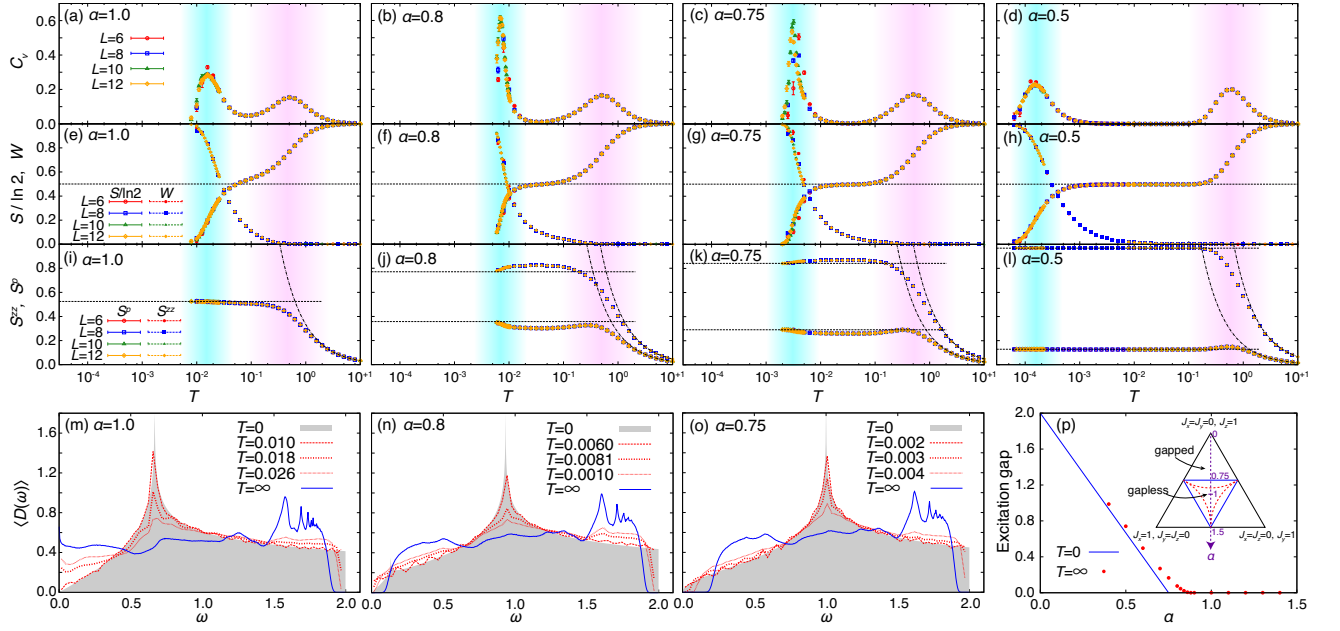


FIG. 1: (color online). (a)-(d)  $T$  dependences of the specific heat at (a)  $\alpha = 1.0$ , (b)  $\alpha = 0.8$ , (c)  $\alpha = 0.75$ , and (d)  $\alpha = 0.5$  in the several clusters with  $2 \times L^2$  spins. Here, we define the anisotropy parameter  $\alpha$  by taking  $J_x = J_y = \alpha/3$  and  $J_z = 1 - 2\alpha/3$ . (e)-(h)  $T$  dependences of the entropy per site,  $S$ , and the thermal average of the density of the flux  $W_p$ ,  $W$ . (i)-(l)  $T$  dependences of the equal-time spin correlations,  $S^{\mu\nu}$ ;  $S^p = (S^{xx} + S^{yy})/2$ . The horizontal dashed lines represent the values at  $T = 0$  which are calculated analytically [18], and the dashed-dotted curves represent the high- $T$  Curie behaviors  $S^{\mu\nu} \sim J_l/T$ . (m)-(o) The DOS of Majorana fermions at (m)  $\alpha = 1.0$ , (n)  $\alpha = 0.8$ , and (o)  $\alpha = 0.75$ . Except the results at  $T = 0$  and  $T = \infty$ , the DOS are calculated by QMC for the  $10 \times 10$  superlattice of the  $L = 12$  cluster. (p) The excitation gap for the Majorana fermions at  $T = 0$  (blue solid line) and  $T = \infty$  (red symbols) as a function of  $\alpha$ . The inset indicates the gapped-gapless boundaries on the plane of  $J_x + J_y + J_z = 1$ . The blue solid lines represent the phase boundaries in the ground state, while the red dashed lines represent the boundaries obtained from the DOS at  $T = \infty$ . See the text for details.

dence of the Fermi distribution function: we take into account the effect of thermal fluctuations only on  $\eta_r$ . The calculations were done for the  $10 \times 10$  supercell, where the  $L = 12$  cluster obtained by the MC simulation is regarded as a unit cell. The calculations at  $T = 0$  ( $T = \infty$ ) are performed for a  $L = 6,000$  ( $L = 60$ ) cluster. In the calculation at  $T = \infty$ , we take a simple average over 10,000 random configurations of  $\{\eta_r\}$ .

Figure 1(m) shows the DOS of the itinerant Majorana fermion  $c_j$  for the isotropic case  $\alpha = 1.0$  ( $J_x = J_y = J_z$ ). The QMC data are shown near  $T_L$ , together with the results at  $T = 0$  and  $T = \infty$ . In this gapless QSL region, at  $T = 0$ , the DOS shows semimetallic behavior  $D(\omega) \propto \omega$  for small  $\omega$ , reflecting the Dirac dispersion. While increasing  $T$  above  $T_L$ , however, the semimetallic dip of DOS is filled rapidly, leading to “metallic” behavior,  $\langle D(\omega = 0) \rangle \neq 0$ . The result clearly indicates that the thermal fluctuations of fluxes near  $T_L$  significantly affect the low-energy spectrum of itinerant Majorana fermions.

The significant change leads to peculiar behavior in the intermediate- $T$  range between the two crossovers. One is in transport properties. We here show it by computing the optical conductivity of itinerant Majorana fermions, which are mobile carriers in the system. First, we introduce the

Fourier transform of the Hamiltonian as  $\mathcal{H} = \sum_{\mathbf{k}} \mathbf{c}_{\mathbf{k}}^\dagger H_{\mathbf{k}} \mathbf{c}_{\mathbf{k}} = \sum_{n: E_{n\mathbf{k}} > 0} \sum_{\mathbf{k}} E_{n\mathbf{k}} (f_{n\mathbf{k}}^\dagger f_{n\mathbf{k}} - 1/2)$ , where  $\mathbf{c}_{\mathbf{k}}$  is a set of the Fourier transforms of  $c_j$  and the  $L \times L$  cluster is regarded as a unit cell. The Bloch Hamiltonian  $H_{\mathbf{k}}$  is diagonalized by introducing a set of fermions  $f_{n\mathbf{k}}$  belonging to the  $n$ -th band with the energy  $E_{n\mathbf{k}}$ . Then, the conductivity tensor is calculated by  $\sigma^{\mu\nu}(\omega) = \frac{1}{L} \int_0^\infty dt e^{i(\omega+i\delta)t} \int_0^\beta d\lambda \langle J_\nu(-i\lambda) J_\mu(t) \rangle$ , where  $\delta$  is an infinitesimal positive number,  $\mathcal{O}(t) = e^{i\mathcal{H}t} \mathcal{O} e^{-i\mathcal{H}t}$ , and the current operator is defined as  $J_\mu = \sum_{\mathbf{k}n'n} f_{\mathbf{k}n}^\dagger f_{\mathbf{k}n'} \langle u_{\mathbf{k}n} | \partial H_{\mathbf{k}} / \partial k_\mu | u_{\mathbf{k}n'} \rangle$  with the eigenstate  $|u_{\mathbf{k}n}\rangle$  of  $H_{\mathbf{k}}$ . We use the  $1 \times 1$  supercell for the  $\mathbf{k}$  mesh. The inset of Fig. 3 shows the results at several  $T$  for  $\alpha = 1.0$ . The incoherent component at finite  $\omega$  increases with decreasing  $T$  below  $T_H$ . To clarify the contribution to coherent transport, we calculate the Drude weight defined through the sum rule given as  $D_x = \frac{1}{2L} \sum_{\langle ij \rangle_x} \langle J_x \sigma_i^x \sigma_j^x \rangle - \frac{1}{\pi} \int_0^\infty \sigma^{xx}(\omega) d\omega$ , where the summation  $\sum_{\langle ij \rangle_x}$  is taken only for the NN  $x$  bonds on the boundary. Figure 3 shows the  $T$  dependence of  $D_x$ . While decreasing  $T$ , the Drude weight gradually increases below  $T_H$ , and sharply decreases to zero below  $T_L$  after showing a peak near  $T_L$ . The result suggests that the transport quantities, such as the thermal conductivity, have sizable values between the two crossovers.

The significant change in the DOS also results in a pecu-

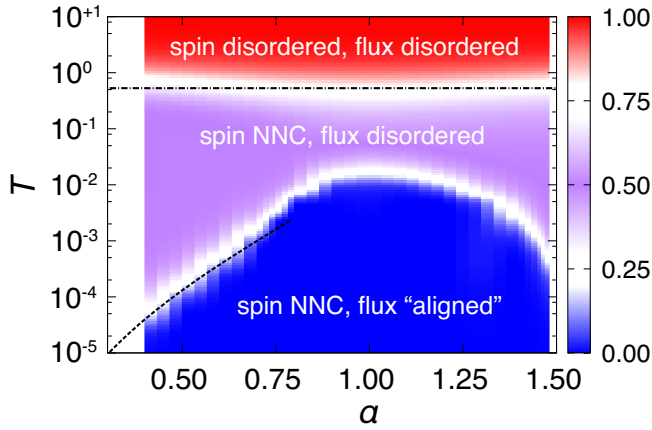


FIG. 2: (color online). Contour map of the entropy per site,  $S/\ln 2$ , on a plane of  $T$  and  $\alpha$ . The dashed line represents crossover temperature obtained by the perturbation theory in the limit of  $J_z \gg J_x, J_y$  ( $\alpha \ll 1$ ). The dashed-dotted line represents the crossover temperature obtained by assuming the constant DOS. NNC stands for a NN correlation.

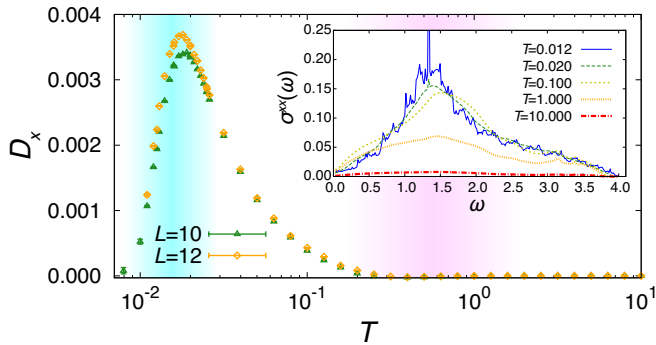


FIG. 3: (color online).  $T$  dependence of the Drude weight of itinerant Majorana fermions at  $\alpha = 1.0$ . The inset shows the optical conductivity at  $\alpha = 1.0$  on the  $L = 12$  cluster at several  $T$ .

liar  $T$  dependence of the specific heat  $C_v$ . In the gapless QSL region, the low- $T$  specific heat is expected to be proportional to  $T^2$  because of the Dirac semimetallic dispersion for aligned fluxes. However,  $C_v$  calculated by assuming all  $\eta_r = +1$  largely deviates from our QMC data in the calculated  $T$  range, as shown for  $\alpha = 1.2$  in Fig. 4. This indicates that the asymptotic  $T^2$  behavior will be limited only in the extremely low- $T$  region, much lower than  $T_L$ . In a wide range of  $T_L \lesssim T \lesssim T_H$ , however, we find that  $C_v$  well scales to  $\propto T$ , which originates from the “metallic” DOS caused by thermally fluctuating fluxes above  $T_L$ . Furthermore, the overall behavior including  $T \gtrsim T_H$  is well explained by the result for completely random  $\{\eta_r\}$ , as shown in Fig. 4. Thus, as a consequence of the thermal fractionalization of quantum spins, we find the apparent  $T$ -linear behavior, not  $T^2$ , in the region where the NN spin correlations are well developed.

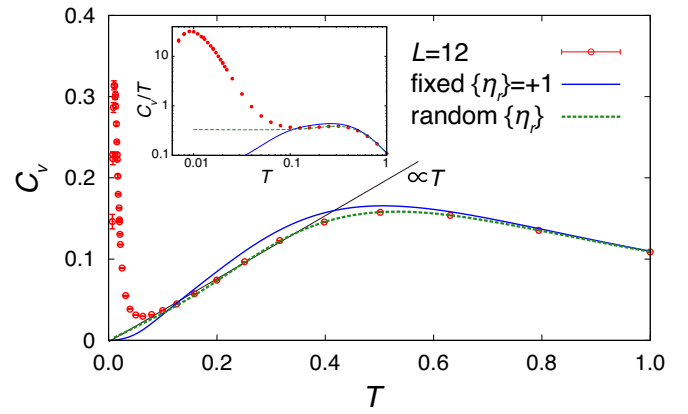


FIG. 4: (color online).  $T$  dependence of the specific heat  $C_v$  at  $\alpha = 1.2$  in the  $L = 12$  cluster. For comparison, the results calculated by fixing all  $\eta_r$  to  $+1$  and by assuming random  $\{\eta_r\}$  are shown as the solid and dashed curves, respectively. The log plot of  $C_v/T$  is also shown in the inset.

Whereas the coherent transport and the  $T$ -linear behavior are observed widely in the region where the ground state is gapless, it is disturbed in the vicinity of the gapped-gapless phase boundary at  $\alpha = 0.75$ . Figures 1(n) and 1(o) show the DOS of the itinerant Majorana fermions at  $\alpha = 0.8$  and  $\alpha = 0.75$ , respectively. At these parameters, the system develops an energy gap with increasing  $T$  in the vicinity of  $T_L$ , in sharp contrast to the gap filling in Fig. 1(m). The schematic phase diagram, determined by the gaps at  $T = 0$  and  $T = \infty$ , is presented in Fig. 1(p). Remarkably, the gapped-gapless boundary is similar to that in the dynamical phase diagram [22] and for the full flux state [23]. The modification of the boundary at finite  $T$  implies that effective exchange couplings are renormalized in an anisotropic way by the thermal fluctuation of localized Majorana fermions. Indeed, the anisotropy of spin correlations is slightly enhanced near  $T_L$  while increasing  $T$ , as shown in Figs. 1(j) and 1(k).

In summary, we have clarified that the thermal fractionalization of quantum spins into Majorana fermions in the Kitaev model manifests itself in experimentally measurable quantities, such as spin correlations, specific heat, and transport properties. The present results will stimulate the experimental hunting of Majorana fermions in quantum magnets, e.g., iridium oxides [24–28] and ruthenium compounds [29–32], where Kitaev-type interactions are expected.

This work is supported by Grant-in-Aid for Scientific Research, the Strategic Programs for Innovative Research (SPIRE), MEXT, and the Computational Materials Science Initiative (CMSI), Japan. Parts of the numerical calculations are performed in the supercomputing systems in ISSP, the University of Tokyo.

- 
- [1] S. Tomonaga, *Prog. Theor. Phys.* **5**, 544 (1950).
- [2] X. G. Wen, *Phys. Rev. B* **44**, 2664 (1991).
- [3] Z. Nussinov, C. D. Batista, B. Normand, and S. A. Trugman, *Phys. Rev. B* **75**, 094411 (2007).
- [4] B. Normand and Z. Nussinov, *Phys. Rev. Lett.* **112**, 207202 (2014).
- [5] C. Castelnovo, R. Moessner, and S. L. Sondhi, *Nature* **451**, 42 (2008).
- [6] V. J. Emery and S. Kivelson *Phys. Rev. B* **46**, 10812 (1992).
- [7] A. Kitaev, *Ann. Phys.* **321**, 2 (2006).
- [8] G. Jackeli and G. Khaliullin, *Phys. Rev. Lett.* **102**, 017205 (2009).
- [9] H.-D. Chen and J. Hu, *Phys. Rev. B* **76**, 193101 (2007).
- [10] X.-Y. Feng, G.-M. Zhang, and T. Xiang, *Phys. Rev. Lett.* **98**, 087204 (2007).
- [11] H.-D. Chen, and Z. Nussinov, *J. Phys. A Math. Theor.* **41**, 075001 (2008).
- [12] J. Chaloupka, G. Jackeli, and G. Khaliullin, *Phys. Rev. Lett.* **105**, 027204 (2010).
- [13] J. Reuther, R. Thomale, and S. Trebst, *Phys. Rev. B* **84**, 100406 (2011).
- [14] J. Chaloupka, G. Jackeli, and G. Khaliullin, *Phys. Rev. Lett.* **110**, 097204 (2013).
- [15] J. Nasu, T. Kaji, K. Matsuura, M. Udagawa, and Y. Motome, *Phys. Rev. B* **89**, 115125 (2014).
- [16] J. Nasu, M. Udagawa, and Y. Motome, *Phys. Rev. Lett.* **113**, 197205 (2014).
- [17] J. Nasu, M. Udagawa, and Y. Motome, *J. Phys.: Conf. Ser.* **592**, 012115 (2015).
- [18] G. Baskaran, S. Mandal, and R. Shankar, *Phys. Rev. Lett.* **98**, 247201 (2007).
- [19] K. P. Schmidt, S. Dusuel, and J. Vidal, *Phys. Rev. Lett.* **100**, 057208 (2008).
- [20] J. Vidal, K. P. Schmidt, and S. Dusuel, *Phys. Rev. B* **78**, 245121 (2008).
- [21] K. Hukushima and K. Nemoto, *J. Phys. Soc. Jpn.* **65**, 1604 (1996).
- [22] J. Knolle, D. L. Kovrizhin, J. T. Chalker, and R. Moessner, *Phys. Rev. Lett.* **112**, 207203 (2014).
- [23] V. Lahtinen, G. Kells, A. Carollo, T. Stitt, J. Vala, J. K. Pachos, *Ann. Phys.* **323**, 2286 (2008).
- [24] Y. Singh and P. Gegenwart, *Phys. Rev. B* **82**, 064412 (2010).
- [25] Y. Singh, S. Manni, J. Reuther, T. Berlijn, R. Thomale, W. Ku, S. Trebst, and P. Gegenwart, *Phys. Rev. Lett.* **108**, 127203 (2012).
- [26] S. K. Choi, R. Coldea, A. N. Kolmogorov, T. Lancaster, I. I. Mazin, S. J. Blundell, P. G. Radaelli, Y. Singh, P. Gegenwart, K. R. Choi, S.-W. Cheong, P. J. Baker, C. Stock, and J. Taylor, *Phys. Rev. Lett.* **108**, 127204 (2012).
- [27] R. Comin, G. Levy, B. Ludbrook, Z.-H. Zhu, C. N. Veenstra, J. A. Rosen, Y. Singh, P. Gegenwart, D. Stricker, J. N. Hancock, D. van der Marel, I. S. Elfimov, and A. Damascelli, *Phys. Rev. Lett.* **109**, 266406 (2012).
- [28] K. Ohgushi, J. I. Yamaura, H. Ohsumi, K. Sugimoto, S. Takeshita, A. Tokuda, H. Takagi, M. Takata, and T. H. Arima, *Phys. Rev. Lett.* **110**, 217212 (2013).
- [29] K. W. Plumb, J. P. Clancy, L. J. Sandilands, V. V. Shankar, Y. F. Hu, K. S. Burch, H. Y. Kee, and Y. J. Kim, *Phys. Rev. B* **90**, 041112 (2014).
- [30] Y. Kubota, H. Tanaka, T. Ono, Y. Narumi, and K. Kindo, *Phys. Rev. B* **91**, 094422 (2015).
- [31] J. A. Sears, M. Songvilay, K. W. Plumb, J. P. Clancy, Y. Qiu, and Y. Kim, arXiv:1411.4610.
- [32] M. Majumder, M. Schmidt, H. Rosner, A. A. Tsirlin, H. Yasuoka, and M. Baenitz, arXiv:1411.6515.